이학석사 학위논문

Statistical evidence for the natural variation of the central Pacific El Niño

중태평양 엘니뇨의 자연변동성에 대한 통계적 증거

2012년 12월

서울대학교 대학원

지구환경과학부

김 진 수

Statistical evidence for the natural variation of the central Pacific El Niño

지도 교수 **Kwang-Yul Kim**

이 논문을 이학석사 학위논문으로 제출함

2012년 12월

서울대학교 대학원

지구환경과학부

김 진 수

김진수의 이학석사 학위논문을 인준함

2012년 12월

위 원 장 _____**(인)**

부위원장 _____**(인)**

위 원 _____**(인)**

Abstract

Statistical evidence for the natural variation of the Central Pacific El Niño

Jin-Soo Kim
School of Earth and Environmental Sciences
The Graduate School
Seoul National University

Extensive studies claimed that the central equatorial Pacific (CP) El Niño has occurred more frequently and strongly than the eastern equatorial Pacific El Niño in recent years. To explain this phenomenon, spatial patterns and principal component time series from several sea surface temperature (SST) data sets in the tropical Pacific are analyzed for the period of 1951–2010. Cyclostationary empirical orthogonal function analysis separates two modes of SST variability, which explain about 50% and 10% of the total SST variability, respectively. Their spatial and temporal patterns are similar among the different SST data sets. The first mode captures the typical El Niño pattern, while the second mode is a dipole pattern in the tropical Pacific. The two modes are, by definition, uncorrelated over the analysis period but are in phase since the late 1990s; superposition of the two modes results in a significant warming in the CP region, which is a potential explanation for a more frequent occurrence of the CP El Niño in the recent decades.

Similar analysis is conducted based on the 500 year data from the Geophysical Fluid Dynamics Laboratory Climate Model version 2.1 under the preindustrial condition. The result is generally consistent with the observations yielding occasional in-phase relationship between the two modes. Thus, it cannot be ruled out that a more frequent occurrence of the CP El Niño in recent years is a natural feature of the equatorial climate system.

Keywords : Central Pacific El Niño, CSEOF, natural variation

Student Number : 2011-20363

Contents

List of tables

List of figures

1. Introduction

El Niño, which is characterized by unusually warm sea surface temperature (SST) in the eastern Pacific and positive and negative sea level pressure anomalies in the western and the eastern Pacific, respectively, is known as a conspicuous phenomenon of ocean-atmosphere interactions in the equatorial climate system [*McPhaden et al*., 2006]. National Oceanic and Atmospheric Administration (NOAA) defines El Niño as the occurrence of 3 month averaged SST anomaly above 0.5℃ in the Niño3.4 region (5ºS–5ºN, 170º–120ºW). Recent studies, however, show that there are different 'flavors' or 'types' of El Niño in terms of their spatial patterns. In many conventional El Niño cases, maximum SST anomaly is observed in the eastern Pacific (hereafter, Eastern Pacific (EP) El Niño). In other cases, however, maximum SST anomaly is observed in the central Pacific rather than the eastern Pacific. This nonconventional type has been referred to as "Dateline El Niño" [*Larkin and Harrison*, 2005a, 2005b], "El Niño Modoki" [*Ashok et al*., 2007], "Central Pacific El Niño" [*Kao and Yu*, 2009], or "Warm pool El Niño" [*Kug et al*., 2009]. Since there is no consensus in the terminology of the nonconventional type of El Niño, it will be called the 'Central Pacific (CP) El Niño' in the present study.

The two types of El Niño have significantly different ocean-atmosphere interactions and different tropics-midlatitude atmospheric teleconnection in both hemispheres [*Weng et al*., 2009; *Song et al*., 2011]. Many recent studies, therefore, investigated why CP El Niño occurs more frequently and strongly during recent years [*Ashok et al*., 2007; *Yu and Kao*, 2007; *Kao and Yu*, 2009; *Kug et al*., 2009; *Yeh et al*.,

2009; *Lee and McPhaden*, 2010]. Despite many recent studies, the reason why CP El Niño is more frequent and stronger in recent years is still unclear.

Climate models, under the anthropogenic greenhouse gas forcing, show a weakening of the trade winds and shoaling of the equatorial thermocline in the central and western Pacific. Therefore, an increasing frequency of the CP El Niño during the recent decade appears to have connection with global warming caused by the anthropogenic forcing [*Yeh et al*., 2009; *Collins et al*., 2010; *Na et al*., 2011]. On the other hand, some studies support that a peculiar trend of the recent CP El Niño is just of natural origin. Using high-quality satellite observations, *McPhaden et al*. [2011] argued that the characteristic of El Niño events has varied naturally and their disparate spatial structures are able to cause change in the background state. Also, *Newman et al*. [2011], using a multivariate red noise approach, argued that the recent change in the occurrence ratios of the two types of El Niño could come from natural variability rather than the anthropogenic forcing. Occurrence ratio of CP El Niño to EP El Niño has been vigorously examined using coupled general circulation models (CGCMs) and the results show that the variation of CP El Niño occurrence is a part of natural climate variability [*Kug et al*., 2010; *Yeh et al*., 2011]. Then, it is debatable whether the global warming or natural variation affects the frequency and the types of El Niño. In this paper, we extract two primary SST patterns from various data sets employing cyclostationary empirical orthogonal function (CSEOF) analysis to explain why the characteristic change of the two types of El Niño has occurred during the past decade.

2. Data and Method

The SST datasets used in this study are the 60-year (1951-2010) NOAA extended reconstruction of historical sea surface temperature version 3 (ERSST V3) [*Smith and Reynolds*, 2004] from the National Climate Data Center, the Met Office Hadley Centre sea ice and sea surface temperature data (HadISST) [*Rayner et al*., 2003], and the 49-year (1958-2006) simple ocean data assimilation reanalysis (SODA) data [*Carton et al*., 2008]. Subsurface temperatures were derived from SODA and precipitations used are the satellite products from Global Precipitation Climatology Project (GPCP) [*Adler et al*., 2003]. Also used was the Geophysical Fluid Dynamics Laboratory (GFDL) Climate Model version 2.1 (CM 2.1) pre-industrial 500-year control dataset [*Delworth et al*., 2006], which was analyzed to understand the CP El Niño in previous studies [*Kug et al*., 2009; *Choi et al*., 2011a, *Choi et al*., 2011b]. At each grid point, monthly mean values were removed from respective months to obtain anomalies from the climatological seasonal cycle.

Recent studies used different methods to separate two types of El Niño: for example, comparison of Niño4 and Niño3 anomalies [*Kug et al*., 2009; *Yeh et al*., 2009; *Yeh et al*., 2011], development of new indices [*Ashok et al*., 2007; *Ren and Jin*, 2011; *Takahashi et al*., 2011], combined EOF analysis [*Kao and Yu*, 2009; *Yu and Kim*, 2010], and red noise approach [*Newman et al*., 2011]. These methods capture the occurrence period of El Niño and Southern Oscillation (ENSO) widely known as 3 to 6 years, but do not resolve physical evolution of ENSO varying with the seasons. In order to resolve

accurate temporal evolution of ENSO, CSEOF analysis was conducted in this study [*Kim et al*., 1996; *Kim and North*, 1997]. As a result, space-time data can be written as

$$P_n(r,t) = \sum_n B_n(r,t)T_n(t), \quad (1)$$

where $P(r,t)$ is raw data, $B_n(r,t)$ are loading vectors (LV), and $T_n(t)$ are principal coefficient (PC) time series. CSEOF LVs are function of time as well as space. Further, CSEOF LVs are periodic in time. Hence,

$$B_n(r,t) = B_n(r,t+d), \quad (2)$$

where d is called the nested period. El Niño cycle has initiation, mature and decay states nearly phase-locked to the seasonal variation of equatorial atmosphere-ocean system; therefore, the nested period was set to be 12 months. As a result, each CSEOF LV describes monthly patterns of physical evolution throughout a year.

We also used regression analysis in CSEOF space to derive physically consistent evolution of subsurface temperatures and precipitation as follows:

$$T_n^{(T)}(t) = \sum_{m=1}^{M} a_m T_m^{(P)}(t) + \varepsilon(t), \quad (3)$$

where $T_n^{(T)}(t)$ is the target PC time series for mode n, a_m and $T_m^{(P)}(t)$ are the regression coefficient and predictor time series for mode m, and $\varepsilon(t)$ is the regression error. The first 20 PC time series ($M = 20$) of a predictor variable are used in (3). In this study, the target variable is 5 m subsurface temperature and the predictor variables are the subsurface temperatures at all vertical levels from the SODA dataset

and also the GPCP precipitation. Then, the regressed patterns of the predictor variable, $R_n^{(PR)}(r,t)$, are obtained as shown in (4):

$$R_n^{(PR)}(r,t) = \sum_{m=1}^{M} a_m R_m^{(P)}(r,t), \quad (4)$$

where $R_m^{(P)}(r,t)$ is the CSEOF LV for mode m of the predictor variable. As a result, spatial patterns of the predictor variable are obtained such that they have (nearly) the same PC time series of the target variable. In this sense, the target patterns $B_n(r,t)$ in (1) and the predictor patterns $R_n^{(PR)}(r,t)$ in (4) are considered physically consistent with each other.

3. Result

3.1. The first two CSEOF modes

Using CSEOF analysis, monthly evolution patterns of the first and the second CSEOF modes were derived from the ERSST (Figure 1); the two modes explain about 50% and 10% of the total SST variance, respectively. The spatial patterns of the first mode are characterized by a basin-scale warming from the eastern Pacific to the central Pacific. Its evolution displays westward growing SST anomalies from the developing stage (June-July-August) to the mature stage (December-January-February). In contrast, the spatial patterns of the second mode exhibit warming in the central Pacific and the western Pacific, and cooling in the eastern Pacific particularly in spring and summer; the major pattern has an appearance of a dipole structure as already discussed in *Ashok et al*.

[2007] and the non-canonical mode in *Guan and Nigam* [2008]. In addition, the eastern Pacific negative SST anomaly develops strongly in boreal spring and summer but disappears in winter. Note that we obtain similar results from the other two SST datasets, i.e., HadISST and SODA (see Figures 2b and 2c).

Figures 2a show the annual mean pattern of the first and the second CSEOF LVs extracted from the ERSST. Similarly, Figures 2b and 2c are for the HadISST and the SODA data. The annual mean patterns of CSEOF LVs are quite similar in all three SST datasets, indicating that the two primary CSEOF modes of SST variability are robust. The regressed subsurface temperature patterns from the SODA dataset are shown in Figure 2d. The first mode shows the opposite signs of subsurface temperature anomalies between the eastern Pacific and the western Pacific, which is associated with the change in thermocline depth [*Kim and Kim*, 2004]. This feature suggests that the thermocline feedback mechanism is associated with the first mode in the eastern Pacific. In contrast, the second mode exhibits smaller scale subsurface warming in the central Pacific, but cooling in the eastern Pacific. The second mode is associated with the thermocline depth in the central and eastern Pacific; this structural difference suggests that the thermocline feedback is less important in the second mode. Moreover, the regressed GPCP precipitation patterns indicate that the atmospheric responses of the two modes are substantially distinct (Figure 2e). These results support that the two modes are physically distinct. In fact, lagged cross-correlation between the two PC time series is less than 0.2 for the lag range of ±24 months.

The PC time series of the datasets are very similar to each other (Figures 3a and

3b). The PC time series of the first mode has a significant spectral peak in a 4-6 year band (figure not shown). The second mode, on the other hand, has a dominant spectral peak in a 7-11 year band. To verify that the first two modes explain the ENSO variability, we compare the Niño indices provided by NOAA and the reconstructed Niño indices based on the two modes (Figures 3c and 3d). The reconstructed indices based on the first two modes of the ERSST dataset are similar to the Niño3 and the Niño4 index as shown in Figures 3c and 3d. One crucial reason why we used the nested period of 12 months is to establish a firm connection of the first two PC time series with the various ENSO indices used in the present study. While using the nested period of 24 months yields physically reasonable modes, i.e., the low-frequency mode and the biennial mode [*Kim*, 2002], the PC time series of the biennial mode has little correlation with both the Niño3 to Niño4 time series. Thus, it is difficult to establish that the first two CSEOF modes represent EP El Niño and CP El Niño, respectively.

Table 1 shows correlations between the CSEOF PC time series and various ENSO indices; to characterize the CP El Niño and the EP El Niño, *Ashok et al*. [2007], *Ren and Jin* [2011] and *Takahashi et al*. [2011] developed new pairs of uncorrelated indices. Correlations of the first PC time series with Niño3 and Niño4 are both significantly high since the first mode exhibits significant loading both in the Niño3 and Niño4 regions. As pointed out in previous studies, Niño3 and Niño4 indices are difficult to explain the observed change in the ENSO statistics [*Ashok et al*., 2007; *Ren and Jin*, 2011; *Takahashi et al*., 2011]. The PC time series of the first mode is significantly related with the N_{CT} index [*Ren and Jin*, 2011] and the C-index [*Takahashi et al*., 2011],

which measures the strength of the EP El Niño. In contrast, the PC time series of the second mode is not strongly related with any indices but the El Niño Modoki Index (EMI) defined by *Ashok et al*. [2007]; this index represents the strength of the CP El Niño. The second PC time series is moderately correlated with the N_{WP} index and the E-index, which also measures the strength of the CP El Niño. These results indicate that CSEOF analysis successfully separate the first two modes of the tropical Pacific SST variability in all the three SST datasets.

Table 1. Correlations between the CSEOF PCs and various ENSO indices for the past 60 years (1951-2010)[a].

	Niño3	Niño4	EMI	N_{CT}	N_{WP}	E-index	C-index
First mode	0.82	0.80	0.30	0.74	0.54	0.51	0.76
Second mode	0.11	0.37	0.75	0.25	0.58	0.57	0.42

[a]EMI is El Niño Modoki Index (SST averaged over (165°E-140°W×10°S-10°N) – 0.5×SST averaged over (110°W-70°W×15°S-5°N)–0.5×SST averaged over (125°E-145°E×10°S-20°N) [*Ashok et al*., 2007]. Cold Tongue El Niño index (N_{CT}; Niño3 – 0.4×Niño4) and Warm Pool El Niño index (N_{WP}; Niño4 – 0.4×Niño3) are defined in *Ren and Jin* [2011]. Eastern Pacific El Niño index (E-index; Niño12 – 0.5×Niño4) and central Pacific El Niño index (C-index; 1.7×Niño4 – 0.1×Niño12) are defined in *Takahashi et al.* [2011].

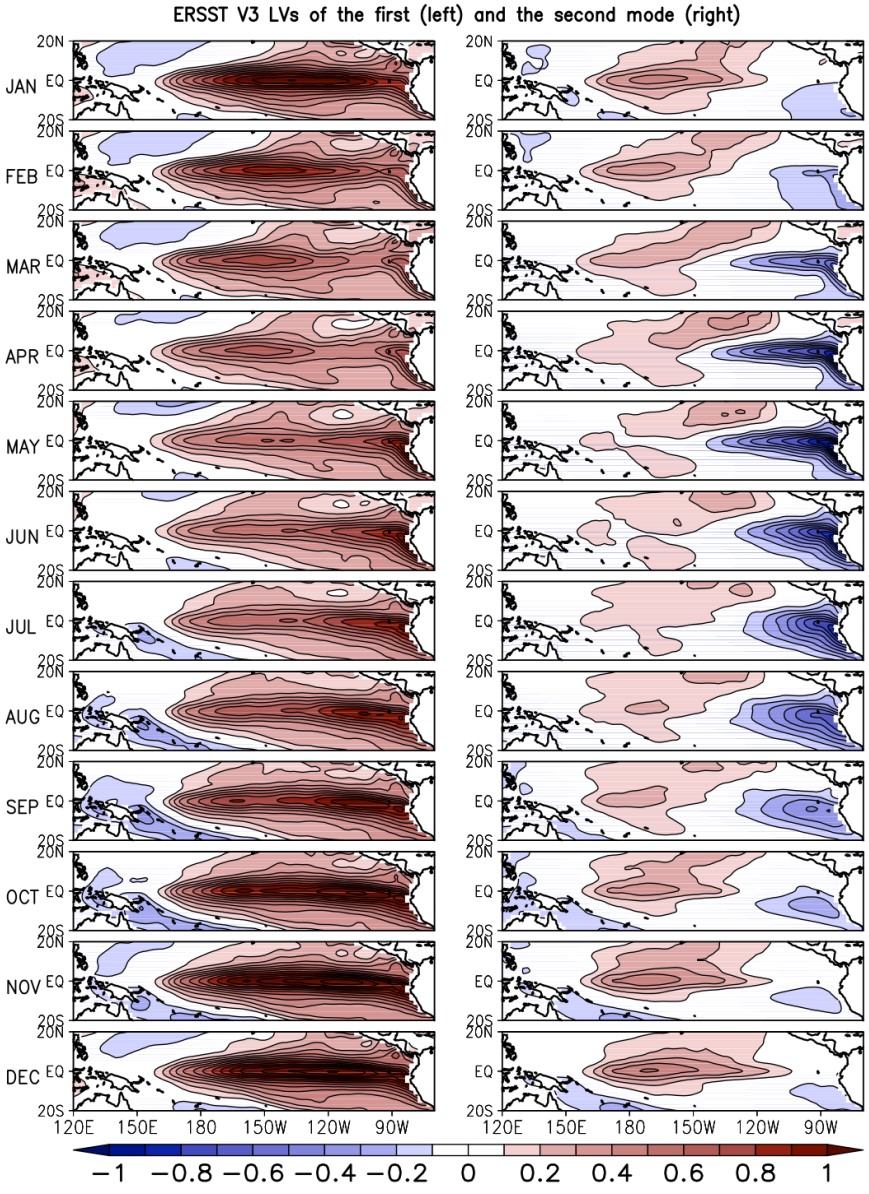

Figure 1. CSEOF LVs of the first (left) and the second (right) modes extracted from the ERSST V3 dataset. Contour interval is 0.1℃.

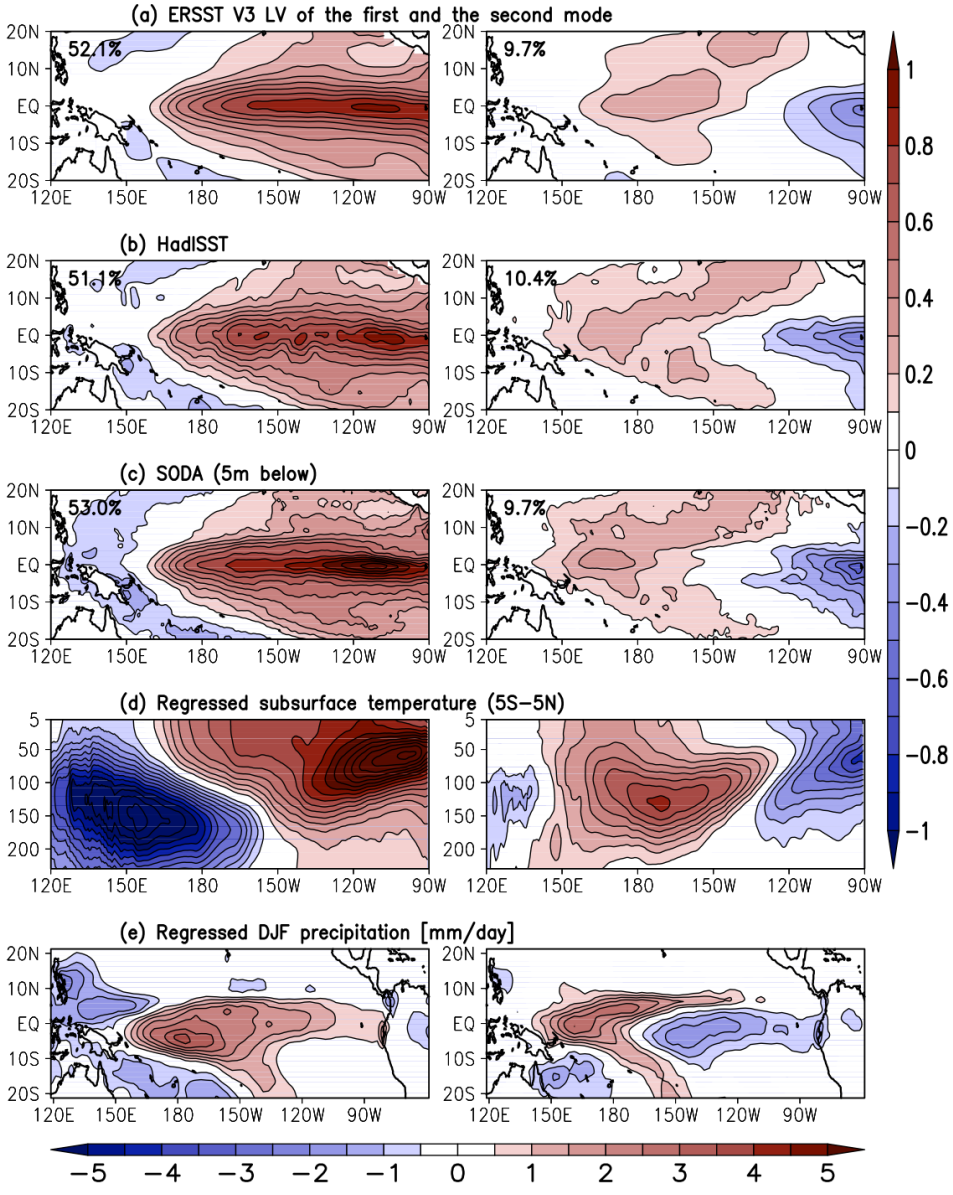

Figure 2. Annually averaged CSEOF LVs of the first (left) and the second (right) modes extracted from (a) ERSST V3, (b) HadISST, and (c) SODA datasets. (d) The regressed field of SODA subsurface temperature averaged over 5°S-5°N. Contour interval is 0.1°C. (e) The regressed patterns of GPCP precipitation. Contour interval is 0.2 mm day^{-1}.

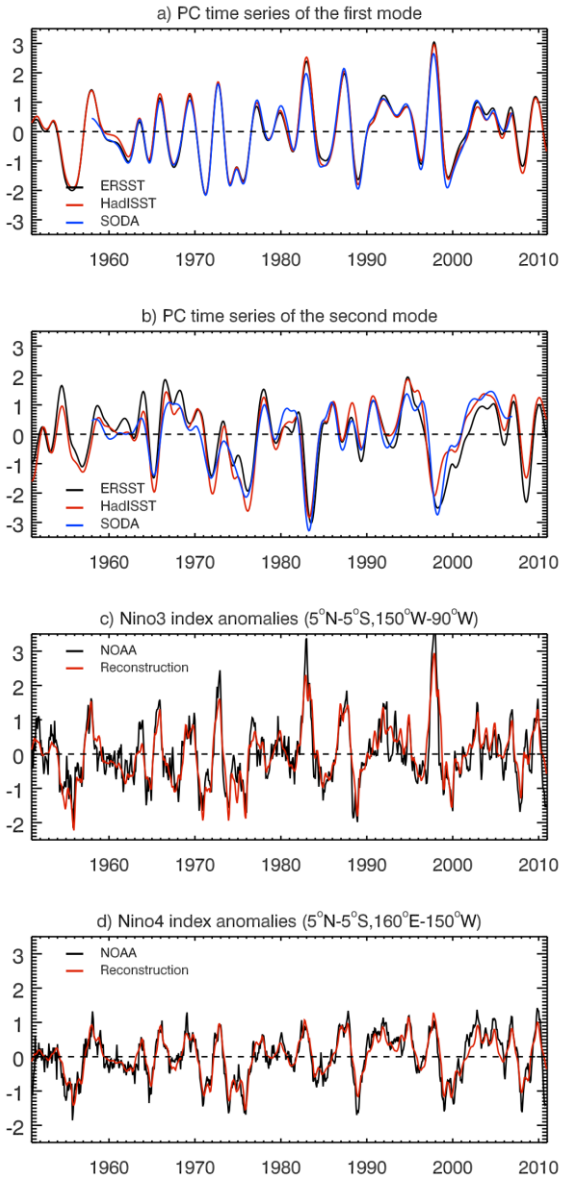

Figure 3. PC time series of (a) the first and (b) the second CSEOF modes from the observational datasets. (c) Niño3 and (d) Niño4 index anomalies from NOAA (black) and the reconstruction SST anomalies based on the first two CSEOF modes (red).

3.2. Changing relationship between the first two CSEOF modes

By definition, the PC time series of the two CSEOF modes are nearly independent and they exhibit little lead-lag relationship in the entire analysis period (not shown here). However, sliding correlation with a 10-year window shows that the relationship between the two modes undergoes significant long-term variations. Since the late 1990s, the two modes exhibit a strong in-phase relationship. To examine the characteristic temporal relationship of the two modes on a low-frequency time scale, sliding correlation of the two PC time series is calculated with a 10-year window (Figure 4). The sliding correlation reveals strong decadal variations with significant positive and negative correlations. It is striking that the sliding correlation increases rapidly to 0.87 since the late 1990s in the HadISST and the ERSST datasets. This indicates that the PC time series of the two modes had varied coherently during the recent decade. As a result, a superposition of the first and the second CSEOF modes with the same sign during the recent decade (see Figures. 3a and 3b) yields a significant warming in the central Pacific but a weak warming in the eastern Pacific. It is argued that the strengthening of the in-phase relationship of the first two CSEOF modes can be a plausible explanation for stronger and more frequent CP El Niños in the recent decade.

In case of 1982/83 and 1997/98 El Niño, the PC time series of the two CSEOF modes are of opposite signs, i.e., positive for the first CSEOF mode and negative for the second mode. The resulting spatial patterns, therefore, appear to be a canonical EP El Niño with a significant warming in the eastern Pacific. Thus, the second mode as well as the first mode contributes significantly to the development of a strong EP El Niño. Not

surprisingly, the average amplitude of the first PC time series during boreal winter (DJF) is 1.38 for EP El Niño years (Table 2), but that of the second PC time series is -0.26; this is a favorable condition for canonical EP El Niños. In contrast, the average amplitudes of the first and the second PC time series are respectively 0.65 and 1.04 during DJF for CP Niño years (Table 2), which is a favorable condition for CP El Niños.

Figure 5 displays the composite evolution patterns averaged over 5°S-5°N of the El Niño events (see Table 2) before and after 2000. The SST anomalies in the top panel are based on the first two modes by multiplying their LVs with corresponding PCs as in (1). The bottom panels are based on the actual SST anomalies. Both the actual and the reconstructed SST anomalies show that the center of anomalous SST is located in the central Pacific after 2000, whereas it is located in the EP before 2000. In addition, anomalous SST before 2000 exhibits westward phase propagation with time, which is not seen after 2000. Varying temporal relationship of the two modes causes these evolutionary differences of El Niños before and after 2000. This is an additional support for the in-phase relationship between the two CSEOF modes being the primary reason for more frequent occurrence of CP El Niño since the year 2000.

Figure 6 shows the DJF mean SST anomalies in the Niño3 and the Niño4 regions for the EP El Niño and the CP El Niño years (Table 2). In Figures 6a and 6b, the first column indicates the DJF Niño3 or Niño4 indices provided by NOAA, the second and the third columns represent the reconstructed Niño3 or Niño4 indices based on the first and the second CSEOF modes, respectively. In Figure 6a, the median values are similar for the first and the second columns while that of the third column is nearly zero;

the first mode explains a significant fraction of Niño3 anomalies while the second mode explains little of the Niño3 anomalies. In contrast, Niño4 index cannot be explained by the first mode alone in CP El Niño years; the second mode explains a significant part of SST variability in the Niño4 region in CP El Niño years. The second mode is as important as the first mode in explaining the occurrence of CP El Niño. While the first mode essentially dictates the occurrence of El Niño or La Niña in the eastern Pacific and its contribution is significantly larger than the second mode, the second mode is essential in determining the central location of ENSO thereby discriminating EP El Niño and CP El Niño.

Table 2. EP and CP El Niño years[a].

	Years
EP	1957-1958, 1963-1964, 1965-1966, 1969-1970, 1972-1973, 1976-1977, 1982-1983, 1986-1987, 1991-1992, 1997-1998 (10 years)
CP	1958-1959, 1968-1969, 1977-1978, 1979-1980, 1987-1988, 1994-1995, 2002-2003, 2004-2005, 2006-2007 (9 years)

[a]El Niño years are defined as the years with DJF averaged SST anomaly above 0.5°C in the Niño3.4 region. EP El Niño is considered to have occurred when Niño3 is greater than Niño4. However, CP El Niño is considered to have occurred when Niño4 is greater than Niño3.

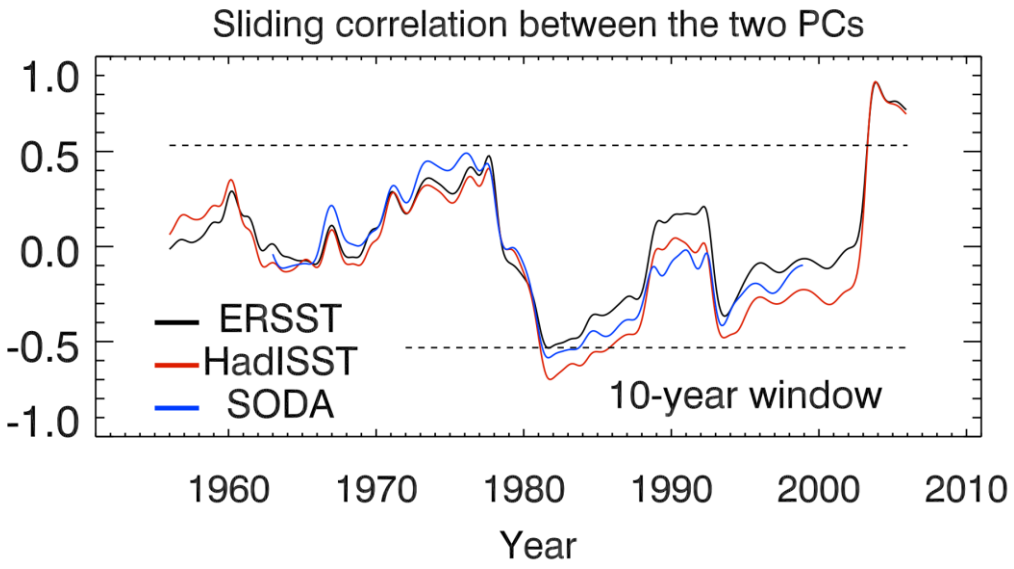

Figure 4. Sliding correlations between the first and the second PC time series with a 10-year window. Dashed lines denote the 95% significance level based on the *t*-test.

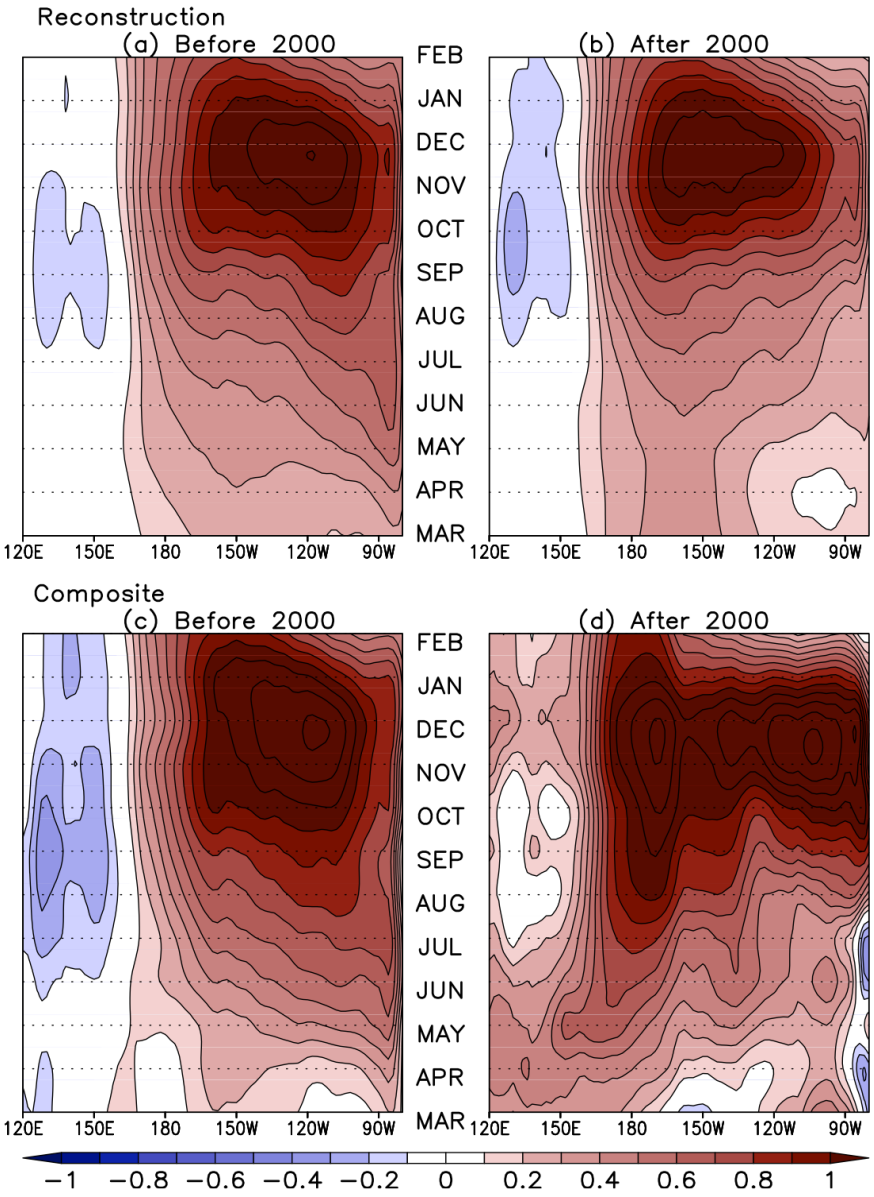

Figure 5. (upper panel) Composite maps of SST anomalies averaged over 5°S-5°N in El Niño years before 2000 (left) and after 2000 (right) based on the reconstructed SST anomalies using the first two CSEOF modes. (lower panel) Composite maps of SST anomalies averaged over 5°S-5°N in El Niño years before 2000 (left) and after 2000 (right) based on the actual data. Contour interval is 0.1℃.

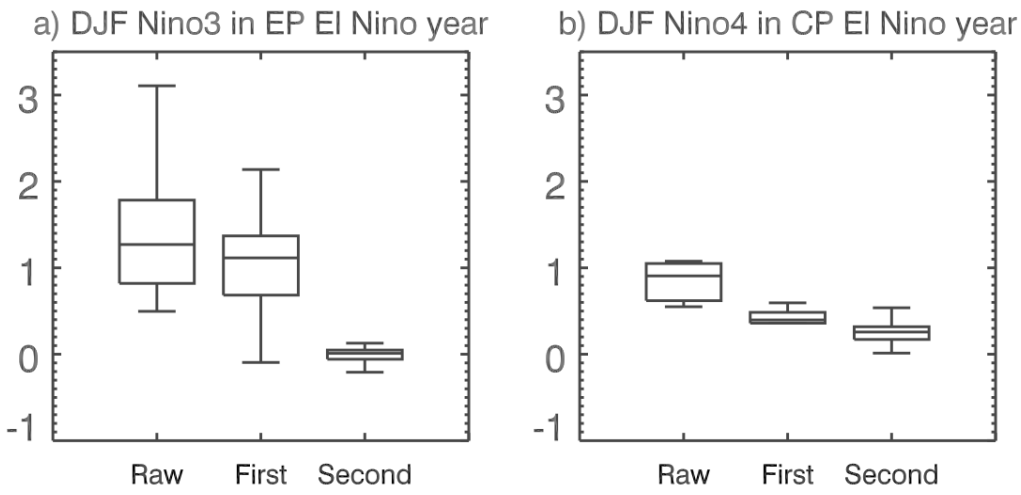

Figure 6. Box plot of (a) DJF Niño3 in EP El Niño years and (b) DJF Niño4 index in CP El Niño years. The first column represents the raw data, the second and the third columns represent the first two CSEOF modes, respectively. Each column shows maximum, minimum, the first, the second (median) and the third quartile values of SST anomalies in Celsius.

3.3. GFDL model results

Because of the relatively short length of the observational datasets, the varying relationship of the two modes needs to be confirmed from a long coupled GCM simulation. Several studies show that the two types of El Niño are captured well in the GFDL model [*Kug et al*., 2009; *Choi et al*., 2011a; *Choi et al*., 2011b]. Therefore, this model is used to examine the hypothesis above.

The spatial patterns and the PC time series of the first (62.3%) and the second (10.7%) modes were extracted from the GFDL CM2.1 pre-industrial 500-year control run. The first mode captures the EP El Niño pattern and the second mode is characterized by a dipole SST anomaly pattern (Figure 7a). The central locations of the spatial patterns, however, are shifted westward by about 20° compared to those of the observations; this is due to model bias as pointed out by *Kug et al.* [2010]. The subsurface temperature anomaly patterns also show that the first mode is associated with thermocline variability on a basin scale while the second mode is associated with shallower thermocline in the central Pacific (Figure 7b). Despite a westward shift of the SST anomaly patterns, GFDL model results are generally consistent with the observations. The sliding correlation between the two PC time series changes on low-frequency time scales, which further supports that the phase relationship between the two modes undergoes natural variations (black curve in the upper panel of Figure 7c). Not surprisingly, difference between the Niño4-m (5°S-5°N, 140°E-170°W) and the Niño3-m (5°S-5°N, 170-110°W), which represents the CP El Niño occurrence ratio in *Kug et al.* [2010] (black curve in the bottom panel of Figure 7c), coincides reasonably

with the sliding correlation (red curve in the upper panel of Figure 7c). In contrast, the occurrence of extreme EP El Niños, when the Niño3-m is three times or more than the Niño4-m in magnitude, is tied with the out-of-phase relationship between the two modes (figure not shown). This result indicates that the occurrence ratio of the two types of El Niño fluctuates naturally and is strongly associated with the phase relationship between the two modes.

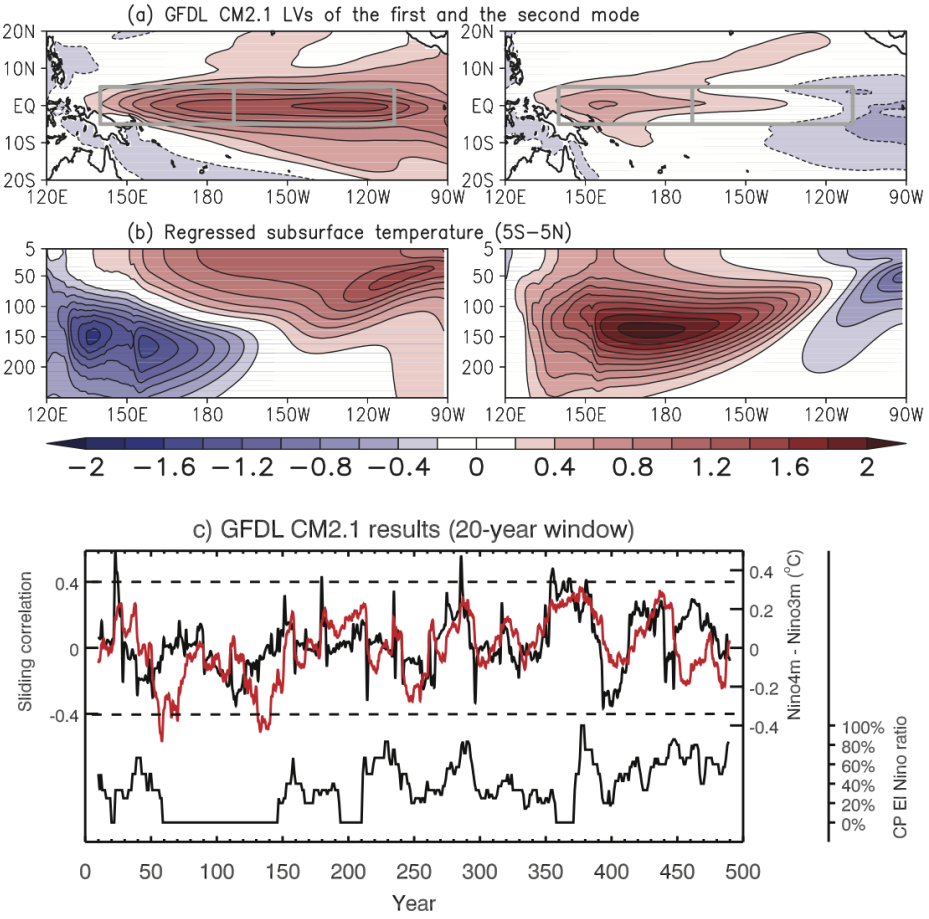

Figure 7. (a) Annually averaged CSEOF LVs of the first and the second modes extracted from the GFDL CM 2.1 500-year run under the pre-industrial conditions. The two gray boxes denote Niño4-m (left) and Niño3-m (right) regions, respectively. (b) The regressed field of subsurface temperature anomalies averaged over 5°S-5°N. Contour interval is 0.2℃ for (a) and (b). (c) (upper panel) Sliding correlation between the first and the second PC time series with a 20-year window (black curve) and the 95% significance level based on the *t*-test (dashed lines). The red curve is the 20-year moving averaged difference between the Niño4-m and the Niño3-m anomalies. (lower panel) The black curve is the 20-year moving averaged CP El Niño occurrence ratio, which is defined as the number of CP El Niños divided by the number of the both types of El Niños. El Niño years are defined as the years of the Niño3.4-m (5°S-5°N, 170°E-130°W) indices being above 0.5°C; CP El Niño is considered to have occurred when Niño4-m is greater than Niño3-m.

4. Conclusion Remarks

There are two dominant and independent SST modes of variability in the equatorial Pacific. The first mode captures well the conventional EP El Niño and the second mode exhibits east-west contrast of SST anomalies. Various “flavors” of El Niño and La Niña can be explained as a varying combination of the two modes. The magnitude of the first mode primarily determines the El Niño state. The second mode, on the other hand, dictates the central location of the SST anomalies. When the PC time series of the second mode is negative, the central location of SST anomalies shifts toward the eastern Pacific and EP El Niño may occur. When the PC time series of the second mode is positive, on the other hand, CP El Niño may occur. Thermocline shallows in the eastern Pacific when the amplitude of the second mode is positive. Since the mean thermocline depth is relatively shallow in the eastern Pacific, there is a limitation in the extent of shoaling.

The in-phase state of the two modes in recent years leads to a more frequent occurrence of CP El Niño. This tendency also appears in long-term model data; this seems to be a fortifying evidence for the natural variation of the frequency of CP El Niño. This in-phase state can be set up by a change in the mean state as reported in several studies [*Yeh et al*., 2009; *Collins et al*., 2010]. In order to confirm this, EOF patterns of the 20-year moving averaged subsurface temperature and regressed SST pattern were calculated (Figure 8) as in *Choi et al* [2011a]. The PC time series of the first mode, which represents the long-term variation of the zonal SST gradient, is highly correlated with the Niño4m-Niño3m time series (Figure 7c); correlation is 0.95. On the

other hand, the second mode, which represents El Niño-like structure [*Choi et al*., 2012], is not significantly correlated with Niño4m-Niño3m time series; correlation is only 0.09. Therefore, tropical decadal variability associated with the ENSO flavor is well connected with the first mode rather than the second mode.

As many previous studies argued, Atlantic Multi-decadal Oscillation (AMO) could contribute to the decadal variability in the tropical Pacific [*Timmermann et al*., 2007; *Zhang and Delworth*, 2007; *Kucharski et al*., 2011]; there are some hint of the AMO signal over the North Atlantic in Figure 8b. The AMO index, averaged SST anomaly for North Atlantic (0°-60°N, 0°-80°W) as defined by *Trenberth and Shea* [2006], exhibits natural fluctuations on low frequency time scales with period greater than 50 years in GFDL-CM2.1 model. Figure 9 shows lagged correlation between the AMO index and the El Niño-related indices. The AMO index and the mean oceanic structure favoring CP El Niño are significantly correlated; the AMO index leads and lags the negative CP El Niño condition by about 50 years. This time scale is known as the AMO period. The regressed fields of the AMO index reveal that the AMO is strongly connected with the first EOF mode of the mean state variability in the Pacific, particularly in the tropics (Figure 10a, 10e). The low frequency oceanic change in the Atlantic can induce variability in the tropical Pacific such as the dipole structure via an atmospheric bridge. As can be seen in the result, the AMO is one plausible mechanism for natural variation of the occurrence frequency of the CP El Niño on multi-decadal time scales. In the historical data, the AMO index and the Niño indices derived from the tree-ring data [*Gray et al., 2004*; *Wilson et al., 2010*] also indicate that the AMO pattern

and the zonal SST gradient in the tropical Pacific are well correlated (Figure 11); the AMO index leads and lags the zonal SST gradient by about 50 years, which is consistent with the GFDL-CM2.1 result (Figure 9). This proxy data support the idea that natural variability in the tropical Pacific is affected by low frequency variability (AMO) in the Atlantic.

Although the model result suggests the natural fluctuation of the CP El Niño frequency in the absence of global warming, observational datasets do not provide concrete evidence. Thus, we cautiously deduce that the recent change in El Niño statistics is caused simply by positive contributions of the two modes rather than external forcing due to global warming. Henceforth, the null hypothesis that the increased occurrence ratio of CP El Niño is due to natural variability cannot be rejected.

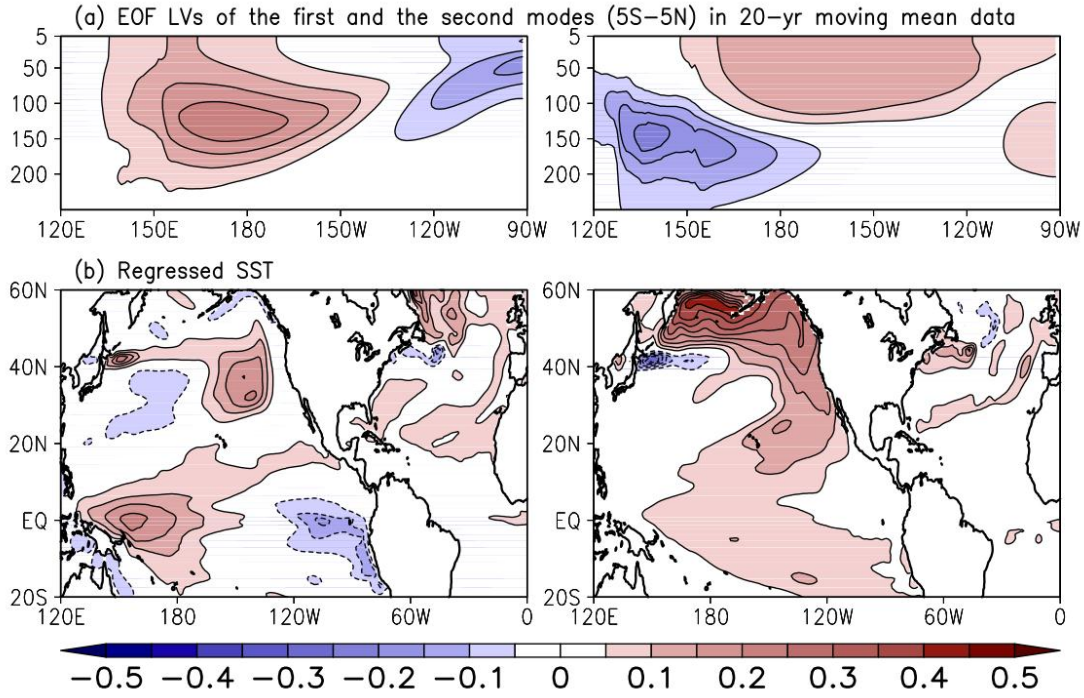

Figure 8. (a) Loading vectors of the first (left) and the second EOF modes (right) extracted from the 20-yr moving averaged subsurface temperatures in the GFDL CM 2.1 500-year run under the pre-industrial condition. Contour interval is 0.05℃. (b) Regressed field of SST anomalies. Contour interval is 0.05℃.

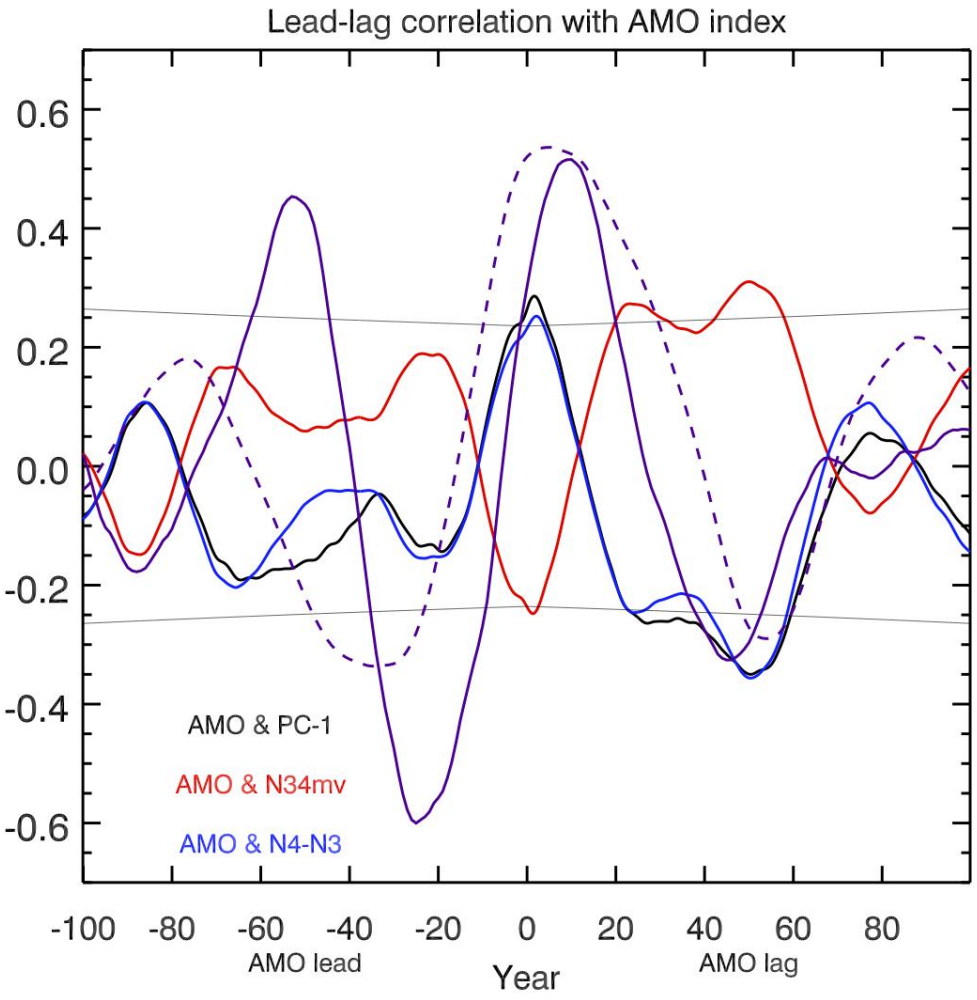

Figure 9. Lead-lag correlation between the AMO index and the first EOF mode in 20-yr moving averaged data (black), moving variance of Niño3.4 (red), and moving averaged Niño4-Niño3 in the GFDL CM 2.1 500-year run under the pre-industrial condition. The 95% significance levels based on the *t*-test are shown (gray). The purple lines indicate correlation of the tree-ring based AMO index with the observational SST (solid) and the tree-ring data (dashed).

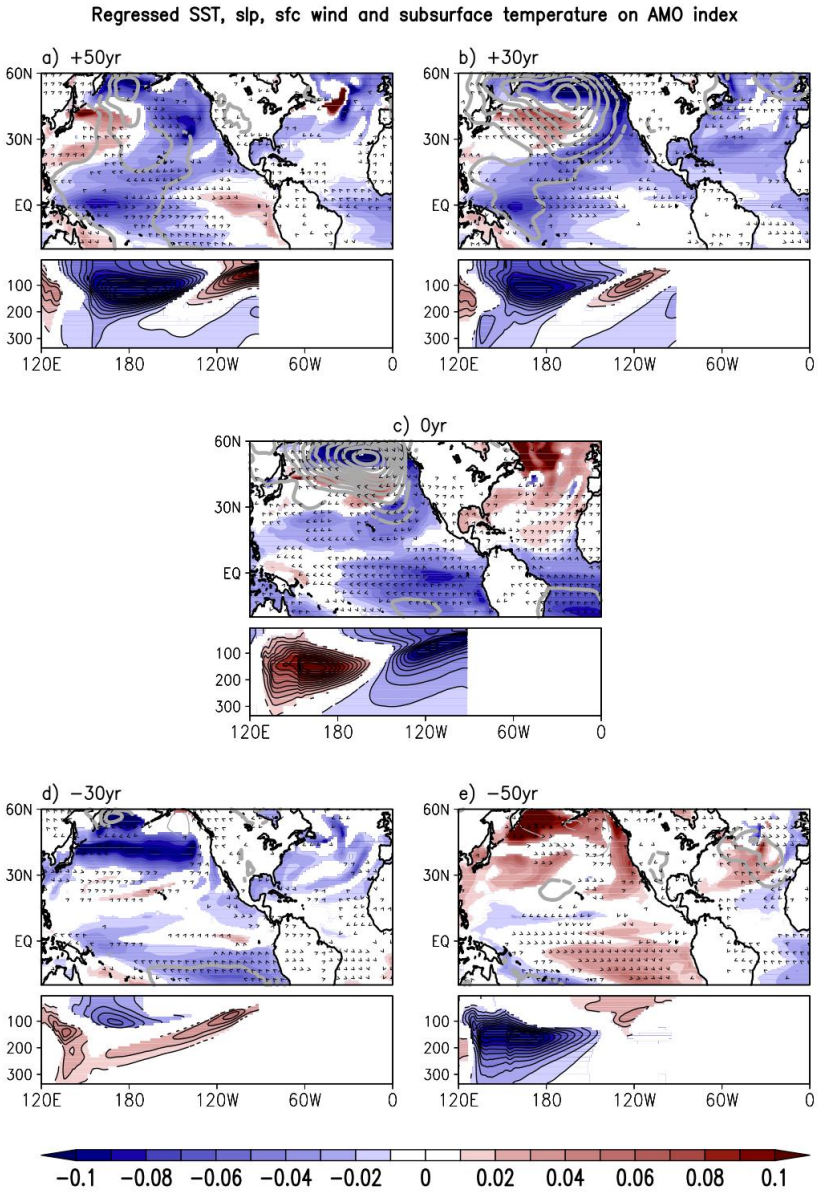

Figure 10. The regressed SST (shaded), sea level pressure (contour), surface wind (vector), and subsurface temperature (the lower panels) at the lag of (a) +50 years, (b) +30 years, (c) 0 year, (d) -30 years, and (e) -50 years with the 20-year smoothed AMO index in the GFDL CM 2.1 500-year run under the pre-industrial condition.

References

Adler, R. F., et al. (2003), The version-2 Global Precipitation Climatology Project (GPCP) monthly precipitation analysis (1979-present), *J. Hydrometeorol., 4(6),* 1147-1167, doi:10.1175/1525-7541(2003)004<1147:TVGPCP>2.0CO;2.

Ashok, K., S. K. Behera, S. A. Rao, H. Weng, and T. Yamagata (2007), El Niño Modoki and its possible teleconnection, *J. Geophys. Res*., *112*, C11007, doi:10.1029/2006JC003798.

Carton, J. A., and B. S. Giese (2008), A reanalysis of ocean climate using Simple Ocean Data Assimilation (SODA), *Mon. Weather Rev*., *136*, 2999–3017, doi:10.1175/2007MWR1978.1.

Choi J., S.-I. An., J.-S Kug., and S.-W. Yeh (2011a), The role of mean state on changes in El Niño's flavor, *Clim. Dyn*., *37*, 1205–1215, doi:10.1007/s00382-010-0912-1.

Choi J., S.-I. An., and S.-W. Yeh (2011b), Decadal amplitude modulation of two types of ENSO and its relationship with the mean state, *Clim. Dyn*., *38*, doi:10.1007/s00382-011-1186-y.

Choi, J., S. An, S. Yeh, and J. Yu (2012), ENSO-like and ENSO-induced Tropical Pacific Decadal Variability in CGCMs., *J. Clim*., doi:10.1175/JCLI-D-12-00118.1, in press.

Collins, M., et al. (2010), The impact of global warming on the tropical Pacific Ocean and El Niño, *Nat. Geosci*., *3*, 391–397, doi:10.1038/ ngeo868.

Delworth, T., et al. (2006), GFDL's CM2 global coupled climate models, part 1: Formulation and simulation characteristics, *J. Clim*., *19*, 643 – 674

Gray, S. T., L. J. Graumlich, J. L. Betancourt, and G. T. Pederson (2004), A tree-ring based reconstruction of the Atlantic Multidecadal Oscillation since 1567 A.D., *Geophys. Res. Lett*., *31*, L12205, doi:10.1029/2004GL019932.

Guan, B., and S. Nigam (2008), Pacific sea surface temperatures in the twentieth century: An evolution-centric analysis of variability and trend, *J. Clim*., *21*, 2790 – 2809, doi:10.1175/2007JCLI2076.1

Kao, H. -Y., and J. -Y. Yu (2009), Contrasting eastern- Pacific and central- Pacific types of ENSO, *J. Clim*., *22*, 615–632, doi:10.1175/2008JCLI2309.1.

Kim, K.-Y. (2002), Investigation of ENSO variability using cyclostationary EOFs of observational data, *Meteor. Atmos. Phys*., *81*, 149-168.

Kim, K.-Y., and Y.-Y. Kim (2004), Investigation of tropical Pacific upper-ocean variability using cyclostationary EOFs of assimilated data, *Ocean Dyn*., *54*, 489 – 505, doi:10.1007/s10236-004-0094-7.

Kim, K.-Y., and G. R. North (1997), EOFs of harmonizable cyclostationary processes, *J. Atmos. Sci.*, *54*, 2416-2427.

Kim, K.-Y., G. R. North, and J. Huang (1996), EOFs of one-dimensional cyclostationary time series: Computations, examples and stochastic modeling, *J. Atmos. Sci.*, *53*, 1007-1017.

Kucharski, F., I.-S. Kang, R. Farneti, and L. Feudale (2011), Tropical Pacific response to 20th century Atlantic warming, *Geophys. Res. Lett*., *38*, L03702, doi:10.1029/

2010GL046248.

Kug, J. -S., F. -F. Jin, and S. -I. An (2009), Two types of El Niño events: cold tongue El Niño and warm pool El Niño, *J. Clim*., *22*, 1499–1515, doi:10.1175/2008JCLI2624.1.

Kug, J. -S., J. Choi, S. -I. An, F. -F. Jin, and A. T. Wittenberg (2010), Warm pool and cold tongue El Niño event as simulated by the GFDL 2.1 coupled GCM, *J. Clim*., 23, 1226-1239, doi:10.1175/2009JCLI3293.1.

Larkin, N. K., and D. E. Harrison (2005a), On the definition of El Niño and associated seasonal average U.S. weather anomalies, *Geophys. Res. Lett*., *32*, L13705, doi:10.1029/2005GL022738.

Larkin, N. K., and D. E. Harrison (2005b), Global seasonal temperature and precipitation anomalies during El Niño autumn and winter, *Geophys. Res. Lett*., *32*, L16705, doi:10.1029/2005GL022860.

Lee, T., and M. J. McPhaden (2010), Increasing intensity of El Niño in the central- equatorial Pacific, *Geophys. Res. Lett*., *37*, L14603, doi:10.1029/2010GL044007.

McPhaden, M. J., S. E. Zebiak, and M. H. Glantz (2006), ENSO as an inte-grating concept in Earth science, *Science*, *314*, 1740–1745, doi:10.1126/science.1132588.

McPhaden, M. J., T. Lee, and D. Mcclurg (2011), El Niño and its relationship to changing background conditions in the tropical Pacific Ocean, *Geophys. Res. Lett*,. 38, L15709 doi:10.1029/2011GL048275.

Na, H., B.-G. Jang, W.-M. Choi, and K.-Y. Kim (2011), Statistical simulations of the future 50-year statistics of cold-tongue El Niño and warm-pool El Niño, *Asia-Pac. J. Atmos. Sci.*, *47*, 223-233.

Newman, M., S.-I. Shin, and M. A. Alexander (2011), Natural variation in ENSO flavors, *Geophys. Res. Lett.*, *38*, L14705, doi:10.1029/ 2011GL047658.

Rayner, N. A., D. E. Parker, E. B. Horton, C. K. Folland, L. V. Alexander,D. P. Rowell, E. C. Kent, and A. Kaplan (2003), Global analyses of sea surface temperature, sea ice, and night marine air temperature since the late nineteenth century, *J. Geophys. Res.*, *108*(D14), 4407, doi:10.1029/2002JD002670.

Ren, H. -L., and F. -F. Jin (2011), Niño indices for two types of ENSO, *Geophys. Res. Lett*., *38*, L04704, doi:10.1029/2010GL046031.

Smith, T. M., and R. W. Reynolds (2004), Improved extended reconstruction of SST (1854–1997), *J. Clim*., *17*, 2466–2477, doi:10.1175/1520-0442(2004)017<2466:IEROS>2.0.CO;2.

Song, H.- J., E. Choi, G.- H. Lim, Y. H. Kim, J.- S. Kug, and S. - W Yeh (2011), The central Pacific as the export region of the El Niño- Southern Oscillation sea surface temperature anomaly to Antarctic sea ice, *J*. *Geophys*. *Res*., *116*, D21113, doi:10.1029/2011JD015645.

Takahashi, K., A. Montecinos, K. Goubanova, and B. Dewitte (2011), ENSO regimes: reinterpreting the canonical and Modoki El Niño, *Geophy. Res. Lett*., *38*, L10704, doi:10.1029/2011GL047364.

Trenberth, K. E., and D. J. Shea (2006), Atlantic hurricanes and natural variability in

2005, *Geophys. Res. Lett*., *33*, L12704, doi:10.1029/2006GL026894.

Timmermann, A., et al. (2007), The influence of a weakening of the Atlantic meridional overturning circulation on ENSO, *J. Clim*., *20*, 4899 – 4919.

Weng, H., S. K. Behera, and T. Yamagata (2009), Anomalous winter climate conditions in the Pacific rim during recent El Niño Modoki and El Niño events, *Clim. Dyn*., *32*, 663–674, doi:10.1007/s00382-008-0394-6.

Wilson, R., et al. (2010), Reconstructing ENSO: The influence of method, proxy data, climate forcing and teleconnections, *J. Quat. Sci*., *25*, 62–78, doi:10.1002/jqs.1297.

Yeh, S. -W., J. -S. Kug, B. Dewitte, M. -H. Kwon, B. P. Kirtman, and F. -F. Jin (2009), El Niño in a changing climate, *Nature, 461*, 511–514, doi:10.1038/nature08316.

Yeh, S. -W., B. P. Kirtman, J. -S. Kug, W. Park, and M. Latif (2011), Natural variability of the central Pacific El Niño event on multi-centennial timescales, *Geophys. Res. Lett*., *38*, L02704, doi:10.1029/2010GL045886.

Yu, J.-Y., and H.-Y. Kao (2007), Decadal changes of ENSO persistence barrier in SST and ocean heat content indices: 1958-2001, *J. Geophys. Res.*, *112*, D13106, doi:10.1029/2006JD007654.

Yu, J. -Y., and S. T. Kim (2010), Identification of central-Pacific and eastern-Pacific types of ENSO in CMIP3 models, *Geophys. Res. Lett*., *37*, L15705, doi:10.1029/2010GL044082.

Zhang, R., and T. L. Delworth (2007), Impact of the Atlantic Multidecadal Oscillation on North Pacific climate variability, *Geophys. Res. Lett*., *34*, L23708,

doi:10.1029/2007GL031601.

초 록

중태평양 엘니뇨의 자연변동성에 대한 통계적 증거

엘니뇨는 해양-대기 상호작용 측면에서 가장 두드러지는 현상으로서 전 세계적으로 여러 이상기상을 초래하는 것으로 잘 알려져 있다. 한편 최근 연구들에 따르면 엘니뇨는 해수면 온도의 변이 값의 중심 위치에 따라 크게 동태평양 엘니뇨와 중태평양 엘니뇨로 구분될 수 있으며, 1990년대 이후에 동태평양 엘니뇨 보다 중태평양 엘니뇨가 더 빈번히 그리고 강하게 발생되고 있다고 보고되었다. 몇몇 학자들은 이러한 관측결과는 지구온난화와 같은 인류발생의 외부강제력에 그 이유가 있다고 주장하였으며, 이와는 반대로 이러한 현상이 단지 자연변동성의 일부일 수 도 있다는 주장도 제기되었다. 이에 본 연구는 이러한 현상을 주성분 분석 방법 중에 하나인 cyclostationary Empirical Orthogonal Function 분석방법을 이용하여, 1951년부터 2010년까지 적도 해수면 온도의 변동을 설명하는 주요한 두 가지 모드를 추출하였으며 그 두 모드로 최근 엘니뇨의 특징을 설명하였다. 첫 번째 해수면 온도 모드는 전체 변동성의 약 50%를 설명하며, 기존에 잘 알려진 동태평양 엘니뇨 기작 및 그에 상응하는 수온약층 되먹임 작용을 잘 나타낸다. 반면, 두

번째 모드는 전체 변동성의 약 10%를 설명하며 적도지역에서 쌍극자형태를 지니고 있어 동태평양과 중태평양의 변이 값의 부호가 반대인 특징을 갖는다. 또한 첫 번째 모드가 겨울철에 큰 변이 값을 갖는 반면에, 두 번째 모드는 봄철 및 여름철에 큰 변이 값을 가지고 있어 완전히 독립적으로 구별되는 물리적 현상이다. 이 두 모드의 주성분의 관계로서 엘니뇨의 다양한 형태가 만들어질 수 있는데, 예를 들어 1982/83, 1997/98의 강한 엘니뇨의 경우 첫 번째 모드는 양의 값을 두 번째 모드는 음의 값을 가져서 두 모드의 효과가 동태평양에 중첩되었기 때문에 강한 엘니뇨가 발달했다고 설명할 수 있고, 라니냐 또한 이와 같이 두 모드의 주성분의 관계로서 설명할 수 있다. 흥미로운 사실은 60년의 기간 동안 서로 독립적인 두 모드의 주성분이 1990년대 후반부터 같은 위상을 가지게 되었다는 사실이다. 이로 인해 중태평양에서는 이 두 모드의 이상 값 효과가 중첩되어 나타나며, 반면에 동태평양에서는 두 모드의 효과가 상쇄도어 나타나게 됨으로써 최근 빈번하게 관측된 중태평야 엘니뇨가 설명될 수 있다. 뿐만 아니라 두 가지 형태의 엘니뇨를 잘 모의한다고 알려진 Geophysical Fluid Dynamics Laboratory Climate Model version 2.1의 산업혁명 이전의 이산화탄소 농도를 활용하여 모의한 500년 기간의 자료를 같은 방법으로 분석한 결과, 서로 독립적인 두 모드가 때때로 십년정도의 시간 스케일에서 같은 위상을 가지는 시점이 관측되며 그 때에 동태평양 엘니뇨에 비해 중태평양 엘니뇨가 더 빈번히 발생한다는 것을 확인하였다. 즉, 자연적으로 독립적인 두 모드가 같은 위상을 가지는 시기가

생길 수 있으며 이 때 동태평양 엘니뇬 보다 중태평양 엘니뇨의 발생 빈도가 유의미하게 클 수 있다는 것이 수치모델 결과에서도 확인 되었다. 따라서 현재 관측되는 엘니뇨의 특성은 자연적인 변동성으로 야기된 것임을 배제할 수가 없다.

주요 용어 : 중태평양 엘니뇨, CSEOF, 자연 변동성
학　　번 : 2011-20363